BULLETIN OF THE POLISH ACADEMY OF SCIENCES
TECHNICAL SCIENCES, Vol. 71(2), 2023, Article number: e144941
DOI: 10.24425/bpasts.2023.144941

Electrospun niobium oxide 1D nanostructures and their applications in textile industry wastewater treatment

Marta ZABOROWSKA*, Weronika SMOK, and Tomasz TAŃSKI

Department of Engineering Materials and Biomaterials, Silesian University of Technology, Konarskiego 18A, 44-100 Gliwice, Poland

Abstract. The textile industry emits daily massive amounts of sewage rich in non-biodegradable organic compounds, especially in textile dyes. Such contaminants are highly soluble in water, which makes their removal difficult. Other studies suggest their carcinogenicity, toxicity, and mutagenicity. A promising chemical treatment of textile wastewater is the photodegradation of dye molecules in the process of photocatalysis in the presence of a photocatalyst. One-dimensional nanostructures exhibit a high surface-to-volume ratio and a quantum confinement effect, making them ideal candidates for nanophotocatalyst material. Nb_2O_5 is gaining popularity in optical applications among other metal oxides with a wide band gap, and electrospun niobium oxide nanostructures, despite their ease and low cost, can increase the chemical removal of textile dyes from wastewater. Facile synthesis of electrospun one-dimensional niobium oxide nanofibers is presented. The nanophotocatalysts morphology, structure, chemical bonds and optical properties were examined. Based on photodegradation of aqueous solutions (ph = 6) of methylene blue and rhodamine B, the photocatalytic activity was established. The photocatalytic efficiency after 180 minutes of ultraviolet irradiation in the presence of Nb_2O_5 nanofibers was as follows: 84.9% and 31.8% for methylene blue and rhodamine B decolorization, respectively.

Key words: electrospinning; niobium oxide; photocatalysis; MB and RhB removal; textile wastewater treatment.

1. INTRODUCTION

The growing problems with the pollution of the aquatic environment encourage scientists to develop efficient methods for wastewater treatment. Today, photocatalytic processes, which are simple and economically advanced oxidation processes (AOPs) that allow for the removal of organic pollutants from water, are among the most important ones [1]. The key to effective photocatalysis is an appropriate photocatalyst, most often semiconductor nanomaterials, among which the most widely researched and used are TiO_2, ZnO, CdS, BiOI [2–8]. Recently, scientists' attention has been focused on photocatalysts based on Nb_2O_5 nanostructures, as indicated by B. Hu *et al.* [9], X. Cui *et al.* [10], A.K. Kulkarni [11] and C. Zhou [12].

Niobium oxide (V) is an n-type semiconductor with a wide band gap depending on the crystal structure ranging from 3.1 to 4.0 eV [13]. Moreover, it is characterized by good chemical and thermal stability, low cost, high corrosion resistance and low toxicity [14, 15]. Additionally, a number of techniques for producing Nb_2O_5 nanostructures are available, including the hydrothermal method [16], solvothermal [17], sol-gel [18], and electrospinning [19]. The latter allows for obtaining one-dimensional Nb_2O_5 nanostructures with a high degree of crystallinity, high specific surface area and no tendency to agglomerate, which are important advantages in the case of photocatalysis. P. Viswanathamurthi *et al.* [19] produced Nb_2O_5 nanofibers with a monoclinic structure using the electrospinning and calcination method at 500, 700°C. M.V. Reddy *et al.* [20] obtained nanofibers from pseudo-hexagonal, orthorhombic (O), and monoclinic (M) Nb_2O_5 phases using the electrospinning method followed by calcination at 500, 800°C, whose superior cycling performance can be used in lithium batteries. Also, J.Y. Cheong *et al.* [21] indicated that the use of electrospinning and calcination at 600°C allows for the production of O–Nb_2O_5 mesoporous nanofibers, which exhibited ultra-stable Li storage characteristics. On the other hand, P. Du *et al.* [22] showed that TiO_2/Nb_2O_5 core-sheath nanofibers produced by coaxial electrospinning and calcination at 500°C, used as an anode in DSSC, provide them with high efficiency of 5.8%. L. Wang *et al.* [23] showed that electrospun nanofibers with the g–C_3N_4/Nb_2O_5 heterojunction are characterized by good photocatalytic activity in the degradation of Rhodamine B (98.1% degradation after 120 min) and phenol (100% degradation after 120 min). L. Wang *et al.* [24] confirmed the high photocatalytic activity of Fe-doped Nb_2O_5 electrospun nanofibers. It was shown that Fe–Nb_2O_5 nanostructures ensured 98.4% degradation of Rhodamine B after 150 min of exposure to visible light.

The lack of extensive research on the photocatalytic activity of one-dimensional Nb_2O_5 nanostructures obtained by the electrospinning method with subsequent calcination prompted the authors to prepare highly-crystalline Nb_2O_5 nanofibers using the above-mentioned method, study their structure, optical properties and efficiency in the photocatalytic decomposition of methylene blue (MB) and rhodamine B (RhB) under the influence of UV light irradiation.

*e-mail: marta.zaborowska@polsl.pl

Manuscript submitted 2022-09-14, revised 2023-01-23, initially accepted for publication 2023-02-27, published in April 2023.

2. MATERIALS AND METHODS

The following materials were used in this paper: ammonium niobate (V) oxalate hydrate (NbO_xA, $NH_4[NbO(H_2O)_2(C_2O_4)_2]\times xH_2O$, purity 99.9%, Pol-Aura), ethanol (EtOH, CH_3CH_2OH, purity 99.8%, Sigma Aldrich), *N*,*N*- dimethylformamide (DMF, purity 99–99.9%, Avantor Performance Materials Poland S.A.), poly(vinylpyrrolidone) (PVP, Mw = 1 500 000 g/mol, Sigma Aldrich), methylene blue (MB, pure, certified, ACROS ORGANICS) and rhodamine B (RhB, pure, certified, ACROS ORGANICS).

As the first step, two solutions of PVP/EtOH and NbOxA/DMF were prepared. The measured amount of poly(vinylpyrrolidone) was added to 7.813 ml of ethanol, to obtain a 10%(wt.) polymer solution. At the same time, 0.5 g of ammonium niobate oxalate hydrate was added to N,N-*dimethylformamide*. Both solutions were subjected to mechanical stirring on magnetic stirrers. After 24 hours, PVP/EtOH and NbOxA/DMF solutions were combined and left for mechanical mixing for further 24 hours (Fig. 1).

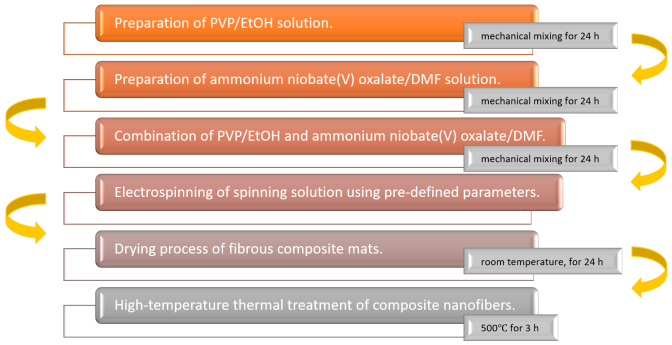

Fig. 1. Scheme of niobium oxide one-dimensional nanostructures preparation method

The final spinning solution PVP/EtOH/NBOxA/DMF was subjected to an electrospinning process on a DOXA Microfluidics Electrospinning Startup Machine device, with the use of the following parameters: the spinning solution flow rate through the nozzle was 0.3 ml/h, the voltage between the nozzle and the collector was set to 18 kV and the distance from the nozzle to the flat collector was 15 cm. Directly after electrospinning, fibrous composite mats were dried overnight at room temperature.

In the last step of Nb_2O_5 1D nanostructures producing method, composite nanofibers were placed in chamber furnace by a Czylok manufacturer, with a heating rate of 5°/minute and final calcination at 500° for 3 hours.

One-dimensional niobium oxide nanostructures were characterized by the studies of morphology using a scanning electron microscope (SEM, Zeiss Supra 25) and structure studies using a transmission electron microscope (TEM, TITAN 80-300, FEI). The microscopes were equipped with a detector facilitating X-ray microanalysis of the elemental composition of electrospun materials (EDX, EDAX). Crystal structure of ceramic nanofibers was performed using a Rigaku MiniFlex 600 (XRD) X-ray diffractometer equipped with a Cu Ka copper tube ($k = 0.15406$ nm) and a D/teX Ultra silicon strip detector. The analysis of the data was made using the Rigaku PDXL software suite. In addition, diffraction patterns of selected micro-areas of samples (SAED) were registered. Structural studies of one-dimensional nanomaterials determining the types of intermolecular interactions and chemical bonds were carried out employing Fourier transform infrared spectroscopy (FTIR, Nicolet ™iS50 by Thermo Scientific ™) in the ATR mode for a wavenumber range of 4000 to 400 cm^{-1} and Raman spectroscopy (Renishaw's Raman in Via Reflex spectrometer) equipped with Leica Research Grade confocal microscope with excitation line of an Ar+ laser source with a wavelength of $\lambda = 514$ nm. The absorbance characteristics in the function of the wavelength of the ceramic one-dimensional niobium oxide were tested using a UV/Vis spectrophotometer (UV/Vis, UV-Vis Evolution 220 by Thermo-Scientific). The study of the specific surface area by nitrogen (N_2) adsorption-desorption method and the analysis of the pore size distribution of calcined nanofibers were carried out on the Gemini VII 5.02 device (Brunauer-Emmett-Teller (BET) method and the Barrett-Joyner-Halenda (BJH) model).

3. RESULTS AND DISCUSSION

3.1. 1D niobium oxide photocatalyst morphology and structure

The analysis of the morphology of ceramic nanofibers was performed using scanning electron microscopy, which demonstrated the highly porous nature of nanostructures, caused by the presence of single crystals building one-dimensional structure in the form of a nanowire (Figs. 2a, b). In addition, uniform diameters of nanofibers were observed along the entire length of the nanostructures, which is a characteristic property of electrospun materials. Based on the scanning electron microscopy (SEM) images, the diameters of the nanostructures were measured and a histogram was drawn showing the distribution of the obtained values. The random measurement of 50 diameters of the fibrous material showed that the material obtained in a three-stage production process had diameters ranging from 125 to approx. 300 nm. The mean value of nanofiber diameters was 190 nm (Fig. 2c).

In order to study the morphology and structure of electrospun niobium oxide nanofibers, analysis was also conducted with the use of transmission electron microscopy in the TEM and high-resolution transmission electron microscopy (HRTEM) modes and the selected area electron diffraction (SAED) micro-area analysis was performed (Figs. 2d,e). The analysis of TEM and HRTEM images confirmed the results obtained on the basis of SEM images – the porous nature of nanofibers, caused by the presence of individual crystals building nanowires. The SAED micro-area analysis showed the monocrystalline nature of individual niobium oxide nanoparticle having T-Nb_2O_5 orthorhombic (Pbam) crystal structure, of which the nanofibers were made (Fig. 2e) [25].

Figure 3 shows the diffraction pattern of the obtained one-dimensional niobium oxide nanostructures. X-Ray diffraction (XRD) analysis revealed the highly crystalline, polycrystalline nature of the nanofibers and the presence of well-defined Miller

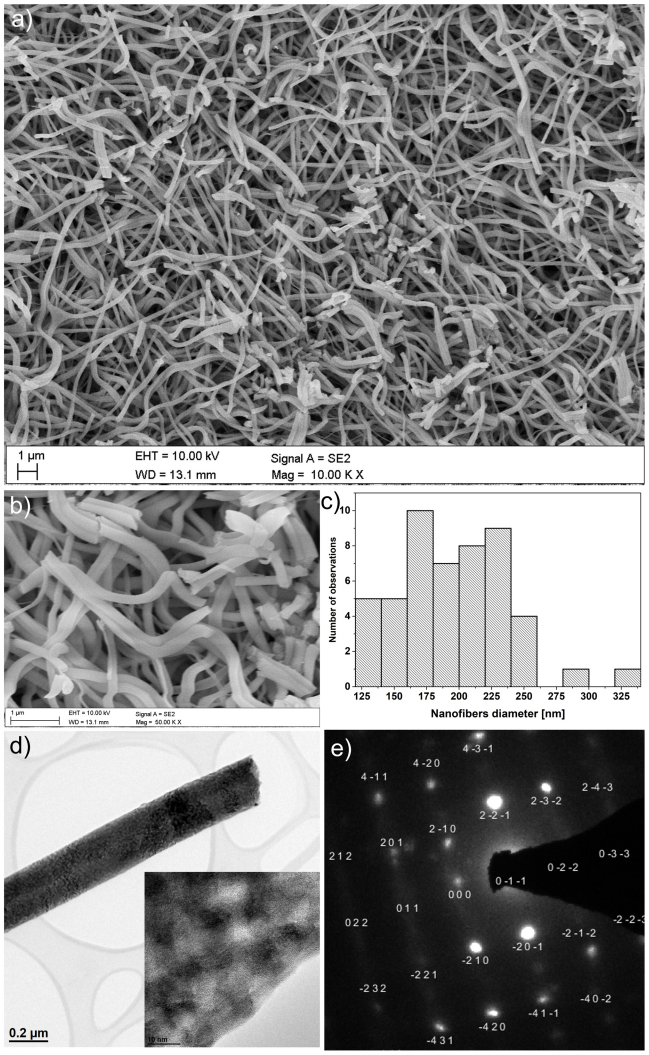

Fig. 2. a) and b) SEM images of Nb_2O_5 calcined nanofibers; c) histogram showing the distribution of 1D nanostructures; d) TEM and HRTEM images of niobium oxide nanofiber; e) SAED of single crystal of electrospun Nb_2O_5 nanofibers

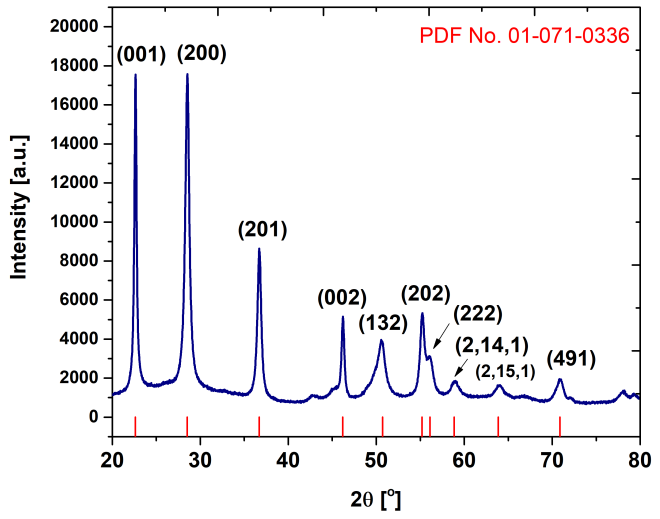

Fig. 3. XRD pattern of 1D niobium oxide nanostructures

indices: (001), (180), (181), (002), (132), (202), (222), (2.14, 1), (2, 15, 1), (491) which correspond to the orthorhombic (Pbam) structure of Nb_2O_5 (according to PDF card no. 01-071-0336). The orthorhombic Nb_2O_5 phase begins to crystallize at 500°C. At this temperature, there may be defects related to atomic diffusion, plane displacements and octahedral distortions of NbO_6, which was also confirmed in subsequent studies using Raman spectroscopy [26].

Moreover, with the use of the Halder–Wagner method, the average size of ceramic crystallites of niobium oxide nanofibers was determined by using the following formulas [27]:

$$\left(\frac{\beta^*}{d}\right)^2 = \frac{1}{D}\frac{\beta^*}{d^2} + \left(\frac{\varepsilon}{2}\right)^2,$$

$$\beta^* = \frac{(\mathrm{FWHM})\cos\theta}{\lambda},$$

$$d = \frac{2\sin\theta}{\lambda},$$

where: λ is the X-ray wavelength, θ is the diffraction angle, FWHM is full width at half peak maximum, ε is the internal stress, and D corresponds to mean crystalline size. Given that the Lorentzian and Gaussian components of the β^* function correspond to the mean crystallite size and stresses, the function takes the form:

$$\left(\frac{\mathrm{FWHM}}{\tan\theta}\right)^2 = \frac{\mathrm{K}\lambda}{D}\frac{\mathrm{FWHM}}{\tan\theta\sin\theta} + \left(\frac{\varepsilon}{2}\right)^2,$$

in which K is constant.

Based on the dependence $(\mathrm{FWHM}/\tan\theta)^2$ vs. $\mathrm{FWHM}/\tan\theta\sin\theta$ the mean crystallite size was determined, taking into account the internal stresses of the niobium oxide crystal lattice, the obtained value was 18.6 nm, and the stress was equal to 0.01.

Niobium (V) oxide has Au and Eu modes visible only in the Fourier-Transform Infrared (FTIR) spectrum and A_g, B_g, E_g modes which are inactive in infrared but active in Raman. Figure 4 shows the FTIR spectrum recorded for the obtained Nb_2O_5 nanofibers. The intense and wide band located at 496 cm^{-1} is assigned to the A_2u mode, which is related to the Nb–O–Nb scissor vibrations of Nb_2O_5 [28, 29]. The second band present in 801 cm^{-1} comes from the E_u mode associated with the O–NbO_4 stretching vibration in the Nb_2O_5 molecule. Moreover, nanofibers do not adsorb water from the air, which is confirmed by the absence of stretching vibration of H_2O molecules in the spectrum.

The Raman spectrum of Nb_2O_5 nanofibers presented in Fig. 4 (inset) is consistent with the one analyzed so far for Nb_2O_5 nanoparticles [30]. The spectrum is dominated by a band around 700 cm^{-1}, which can be attributed to the A_g mode, and it suggests the presence of slightly distorted octahedral NbO_6 species [30]. Less intense bands centered at 120, 230 and 313 cm^{-1} can be attributed to the vibrations of the octahedrons and tetrahedra that build the structure of Nb_2O_5 [31, 32]. The spectroscopic analyses confirmed the SAED results, and

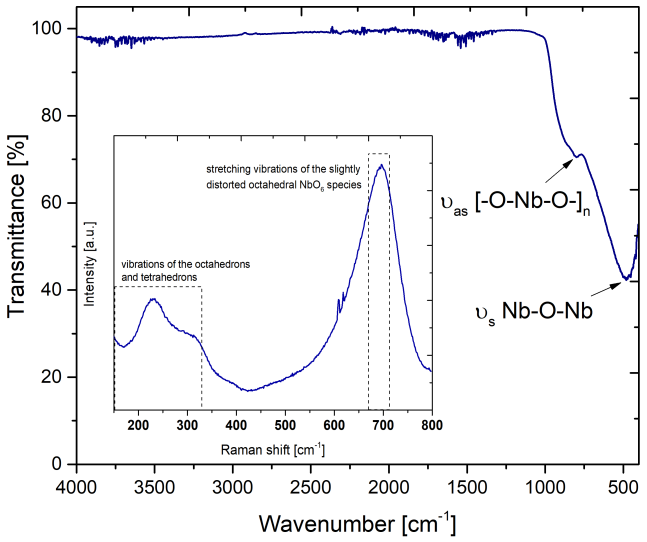

Fig. 4. FTIR and Raman (inset) spectra of one-dimensional niobium oxide nanofibers

the orthorhombic Nb_2O_5 nanofibers produced were devoid of impurities and other phases..

3.2. The specific surface area of Nb_2O_5 nanofibrous mats

One of the key properties of efficient photocatalysts is their specific surface area, which ensures the greatest possible number of catalytically active centers on the surface of the material, accessible to contaminant particles, e.g. dye molecules.

The study of the surface properties of the obtained Nb_2O_5 nanofibers was carried out by analyzing the adsorption-desorption isotherms of nitrogen molecules (N_2) at a constant temperature of 77 K. Figure 5 presents the measurement results on the basis of which it can be concluded that the one-dimensional niobium oxide nanostructures were characterized by a mesoporous nature, as evidenced by the presence of a hysteresis loop on the graph in the range of relative pressure values from 0.6 to 0.9. Moreover, based on the IUPAC classification of porous materials, the shape of the adsorption-desorption curve obtained for niobium oxide nanofibers can be assigned as type IV [33]. The obtained Brunauer-Emmett-Teller (BET) specific surface area of 1D nanostructures of niobium oxide value was 38.54 cm^2/g, which is within the range of values obtained in other studies on electrospun one-dimensional nanomaterials based on niobium oxide [26, 34, 35], and is also significantly higher than the BET value of commercial Nb_2O_5 (3.4804 cm^2/g). Figure 5 (inset) shows pore-size distribution calculated using Barret-Joyner-Halenda (BJH) method. As demonstrated by the pore size distribution graph, most pores were in the range between 5 and 30 nm, and the average value was 7.4 nm. The characteristic mesoporous structure, single crystals building a one-dimensional nanomaterial and a huge specific surface make electrospun fibrous materials an ideal material in photocatalysis processes.

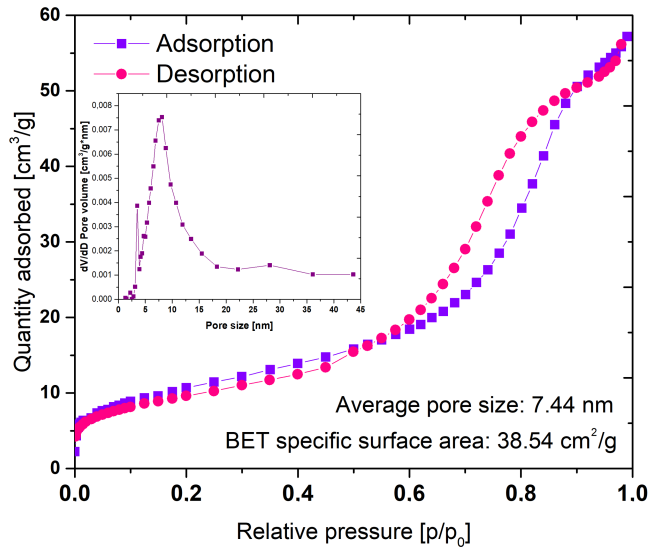

Fig. 5. BET-specific surface area and BJH pore-size distribution (inset) of electrospun niobium oxide nanofibers

3.3. Optical properties of Nb_2O_5-based nanophotocatalyst

The optical properties and energy band gap of the Nb_2O_5 nanofibers were determined based on the graphs of absorption as a function of the wavelength incident on the radiation sample (Fig. 6). The range of electromagnetic radiation absorption for wavelengths from 200 to 800 nm determined for 1D nanostructures showed that this material has a characteristic curve for Nb_2O_5 nanoparticles with an absorption maximum for a wavelength of approx. 210 nm. Using the Tauc dependency, the width of the energy gap of fibrous niobium oxide nanostructures was also determined, i.e. 3.85 eV, which is in line with the Eg Nb_2O_5 (3.1 to 4 eV) range and is also in agreement with other works [26]. The results of the analysis of the optical properties of the photocatalyst in the form of 1D niobium oxide nanostructures indicate a potential application in photocatalysis processes with the use of ultraviolet light.

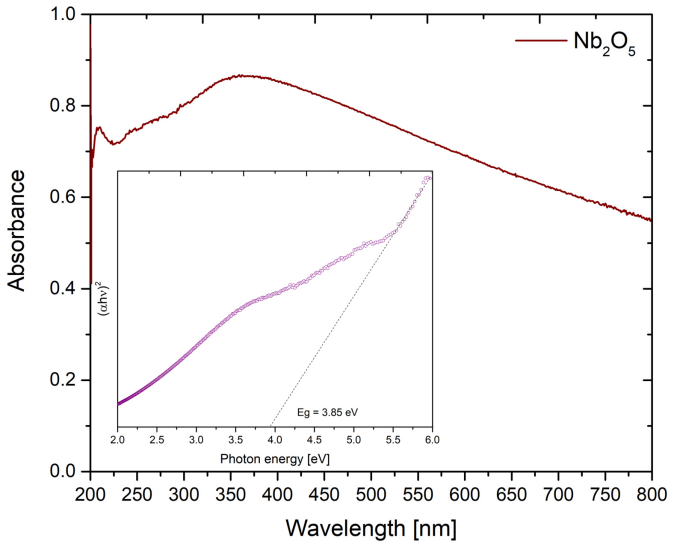

Fig. 6. Dependence of absorbance vs. wavelength and $(\alpha h\nu)^2$ in the function of photon energy (inset) of electrospun Nb_2O_5-based photocatalyst

3.4. Photocatalytic activity studies

The analysis of the photocatalytic activity of one-dimensional niobium oxide nanostructures was performed based on the observations of the photodegradation kinetics of the two most used dyes – methylene blue (MB) and rhodamine B (RhB) under the influence of ultraviolet (UV) radiation with a wavelength of 254 nm. The dyes selected for the study are characterized by good solubility in water and the almost linear dependence of concentration on absorption at their absorption maxima. In order to select the appropriate concentration of dyes in aqueous solutions, in the first stage, the concentration of both dyes – MB and RhB was calibrated. Figure 7 shows the calibration curves of both dyes, on the basis of which the optimal concentrations were selected – 4 ppm for MB and 5 ppm for RhB, which presented the linear dependence of concentration on absorption (Beer–Lambert law).

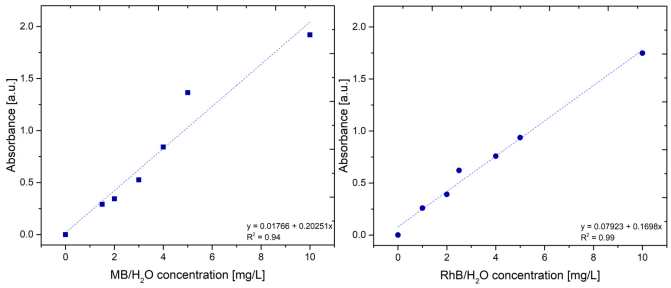

Fig. 7. Calibration curves for aqueous solutions of methylene blue and rhodamine B

Figure 8 shows the decolorization absorption curves of dyes – MB and RhB in their absorption maxima, decreasing as a function of the time of the photodegradation process in the presence of a nanophotocatalyst under the influence of UV radiation and the C/C_0 relationship as a function of photocatalysis time. Based on the measurements conducted for 3 hours, the presence of niobium oxide nanostructures allowed for the decolorization of 84.9% of the initial MB concentration and 31.8% of the RhB concentration. After 30 minutes of dark adsorption, a decrease in MB concentration by 28.5% and RhB concentration by 10% was noted. The significant difference in the degree of decolorization of both dyes is probably due to the chemical nature of MB and RhB particles, which was not affected by the structure of the photocatalyst material.

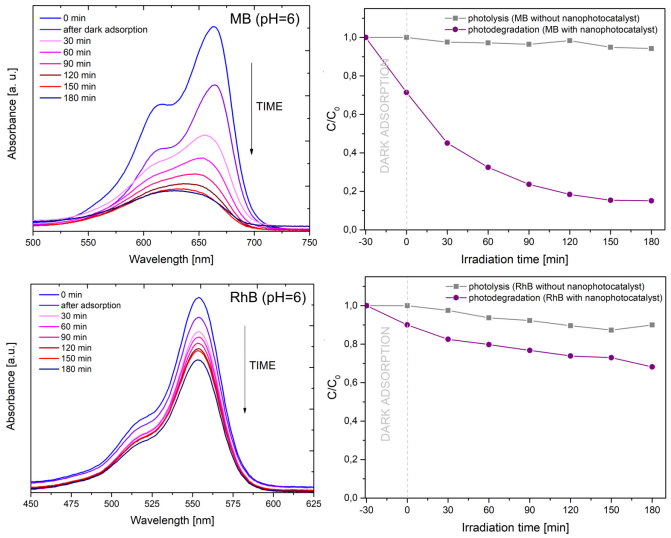

Fig. 8. Decolorization curves of MB and RhB aqueous solutions (pH = 6) in the presence of Nb_2O_5-based nanophotocatalyst

Table 1
Comparison of different niobium oxide photocatalytic activity performance

Material	Catalyst loading [mg/L]	Dye type / Dye concentration [ppm]	Irradiation type	Efficiency [%]/ kinetic rate [min^{-1}]	Ref.
T-Nb_2O_5 nanofibers	1000	MO / 20	UV lamp (300W)	37% in 180 minutes	[36]
TT-Nb_2O_5 hollow spheres	200	IC / 50	UV lamp (100W)	~98% in 80 minutes	[37]
TT-Nb_2O_5 nanorods	NM	MB / NM	UV A lamp	0.0074	[38]
T-Nb_2O_5 submicron particles	100	MB / 50	Solar simulator	59.8% in 60 minutes	[39]
TT-Nb_2O_5 powders	250	MB / 20	UV lamp (150W)	~90% in 150 minutes	[40]
H-Nb_2O_5 powders	1000	MB / 50	UV lamp	~65% in 150 minutes	[41]
Nb_2O_5	1000	BD / 10	UV lamp	22.39% in 24 hours	[42]
T-Nb_2O_5 nanofibers	10	MB / 4	UV lamp (6W)	84.9% in 180 minutes / 0.00949	This work
T-Nb_2O_5 nanofibers	10	RhB / 5	UV lamp (6W)	31.8% in 180 minutes / 0,00163	This work

NM – not mentioned, MO – methyl orange, IC – indigo carmin, MB – methylene blue, RhB – rhodamine B, BD – blue dispersatyl, TT – pseudohexagonal, T – orthorhombic

Similar observations were made in another study [26]. Methylene blue does not possess the –COOH group, which is why it is characterized by a strictly cationic molecular structure, in contrast to rhodamine B. This phenomenon is probably responsible for the different results of photodegradation of both dyes because at the alkaline pH there was a different distribution of the charges of both dyes. The obtained results of photocatalytic activity correspond to the results of other research groups and prove an extremely important thing in the field of photocatalysis – the chemical nature of organic dyes plays a huge role in the observation of the mechanisms of photodegradation reactions of aqueous dye solutions (Table 1). Table 2 shows the first-order kinetic rates of decolorization under the influence of UV radiation in the presence of the nanophotocatalyst of two aqueous solutions MB and RhB. The presence

of one-dimensional niobium oxide nanostructures in the aqueous solution of methylene blue was able to degrade pollutant particles almost 83% faster, compared to the dye particles of rhodamine B solution (pH = 6).

Table 2
First-order kinetic constant of decolorization of MB and RhB aqueous solutions in the presence of Nb_2O_5-based nanophotocatalyst

	MB solution	RhB solution
Kinetics rate [min^{-1}]	9.49×10^{-3}	1.63×10^{-3}

4. CONCLUSIONS

The economical and repeatable electrospinning method from PVP/EtOH/NBOxA/DMF solution was used to prepare highly crystalline niobium oxide nanofibers with an orthorhombic crystal structure confirmed by XRD and FTIR. One-dimensional Nb_2O_5 nanostructures with diameters ranging from 125 to 300 nm of high porosity were tested for the specific surface area using the molecular nitrogen adsorption-desorption isotherms and the obtained value was 38.54 cm^2/g and the average pore size was 7.44 nm. The optical properties of the nanophotocatalyst based on electrospun Nb_2O_5 facilitated the use of UV radiation with a wavelength of 254 nm in the process of photodegradation of dyes – methylene blue and rhodamine B in the presence of a photocatalyst. The obtained results of the dye decolorization degree, MB and RhB respectively, were 84.9% and 31.8%. The conducted research and analysis of the produced nanomaterial confirms the potential use of one-dimensional niobium oxide nanostructures in the processes of water purification from textile dyes. Further research should be done on dye solution conditions (e.g. solution pH), which affect photodegradation kinetic constants.

ACKNOWLEDGEMENTS

Publication supported under the Excellence Initiative – Research University program at the Silesian University of Technology, for years 2021–2022 (pro-quality grant to finance the start-up of activities in new research topics No. 32/014/SDU/10-22-03).

REFERENCES

[1] M.A.U. Olea, J. de J.P. Bueno, and A.X.M. Pérez, "Nanometric and surface properties of semiconductors correlated to photocatalysis and photoelectrocatalysis applied to organic pollutants – A review," *J. Environ. Chem. Eng.*, vol. 9, no. 6, p. 106480, Dec. 2021, doi: 10.1016/J.JECE.2021.106480.

[2] A.H. Zyoud *et al.*, "Removal of acetaminophen from water by simulated solar light photodegradation with ZnO and TiO_2 nanoparticles: Catalytic efficiency assessment for future prospects," *J. Environ. Chem. Eng.*, vol. 8, no. 4, p. 104038, Aug. 2020, doi: 10.1016/J.JECE.2020.104038.

[3] T.L.T. Le, T.H.T. Le, K. Nguyen Van, H. Van Bui, T.G. Le, and V. Vo, "Controlled growth of TiO_2 nanoparticles on graphene by hydrothermal method for visible-light photocatalysis," *J. Sci. Adv. Mater. Devices*, vol. 6, no. 4, pp. 516–527, Dec. 2021, doi: 10. 1016/J.JSAMD.2021.07.003.

[4] A. Manohar *et al.*, "Synthesis and characterization of ZnO nanoparticles for photocatalysis, antibacterial and cytotoxicity in kidney cancer (A498) cell lines," *J. Alloys Compd.*, vol. 874, p. 159868, Sep. 2021, doi: 10.1016/J.JALLCOM.2021.159868.

[5] X. Guo, C. Chen, W. Song, X. Wang, W. Di, and W. Qin, "CdS embedded TiO_2 hybrid nanospheres for visible light photocatalysis," *J. Mol. Catal. A Chem.*, vol. 387, pp. 1–6, Jun. 2014, doi: 10.1016/J.MOLCATA.2014.02.020.

[6] Y. Liu, S. Shen, J. Zhang, W. Zhong, and X. Huang, "Cu2-xSe/CdS composite photocatalyst with enhanced visible light photocatalysis activity," *Appl. Surf. Sci.*, vol. 478, pp. 762–769, Jun. 2019, doi: 10.1016/J.APSUSC.2019.02.010.

[7] Y. Long, Y. Wang, D. Zhang, P. Ju, and Y. Sun, "Facile synthesis of BiOI in hierarchical nanostructure preparation and its photocatalytic application to organic dye removal and biocidal effect of bacteria," *J. Colloid Interface Sci.*, vol. 481, pp. 47–56, Nov. 2016, doi: 10.1016/J.JCIS.2016.07.041.

[8] M. Arumugam *et al.*, "Solvent-mediated synthesis of BiOI with a tunable surface structure for effective visible light active photocatalytic removal of Cr(VI) from wastewater," *Environ. Res.*, vol. 197, p. 111080, Jun. 2021, doi: 10.1016/J.ENVRES.2021.111080.

[9] B. Hu and Y. Liu, "Nitrogen-doped Nb_2O_5 nanobelt quasi-arrays for visible light photocatalysis," *J. Alloys Compd.*, vol. 635, pp. 1–4, Jun. 2015, doi: 10.1016/J.JALLCOM.2015.02.109.

[10] X. Cui, Z. Yang, X. Zhang, W. Liu, B. Zou, and W. Liao, "Fabrication of novel heterojunction of (1D) Nb_2O_5 nanorod/(0D) CdS nanoparticles for efficient removal of U(VI) from water," *Appl. Surf. Sci.*, vol. 599, p. 154027, Oct. 2022, doi: 10.1016/J.APSUSC.2022.154027.

[11] A.K. Kulkarni *et al.*, "In situ preparation of N doped orthorhombic Nb_2O_5 nanoplates /rGO composites for photocatalytic hydrogen generation under sunlight," *Int. J. Hydrogen Energy*, vol. 43, no. 43, pp. 19873–19884, Oct. 2018, doi: 10.1016/J.IJHYDENE.2018.09.013.

[12] C. Zhou *et al.*, "Spatial separation of charge carriers in Nb_2O_5 nanorod superstructures for enhanced photocatalytic H2 production activity," *Mater. Today Chem.*, vol. 10, pp. 259–263, Dec. 2018, doi: 10.1016/J.MTCHEM.2018.09.005.

[13] C.L. Ücker *et al.*, "Influence of Nb_2O_5 crystal structure on photocatalytic efficiency," *Chem. Phys. Lett.*, vol. 764, p. 138271, Feb. 2021, doi: 10.1016/J.CPLETT.2020.138271.

[14] C.L. Ücker *et al.*, "Facile preparation of Nb_2O_5/TiO_2 heterostructures for photocatalytic application," *Chem. Phys. Impact*, vol. 4, p. 100079, Jun. 2022, doi: 10.1016/J.CHPHI.2022.100079.

[15] C.L. Ücker *et al.*, "Photocatalytic degradation of rhodamine B using Nb_2O_5 synthesized with different niobium precursors: Factorial design of experiments," *Ceram. Int.*, vol. 47, no. 14, pp. 20570–20578, Jul. 2021, doi: 10.1016/J.CERAMINT.2021.04.066.

[16] H.M. Wadullah, M. Talib Mohammed, and T. Khalid Abdulrazzaq, "Structure and characteristics of Nb_2O_5 nanocoating thin film for biomedical applications," *Mater. Today Proc.*, vol. 62, pp. 3076–3080, Jan. 2022, doi: 10.1016/J.MATPR.2022.03.229.

[17] P. Zhang *et al.*, "Facile synthesis and characterization of low crystalline Nb_2O_5 ultrafine nanoparticles as a new efficient photocatalyst," *J. Non. Cryst. Solids*, vol. 500, pp. 371–376, Nov. 2018, doi: 10.1016/J.JNONCRYSOL.2018.08.026.

[18] G. Taques Tractz, F. Staciaki da Luz, S. Regina Masetto Antunes, E. do Prado Banczek, M. Taras da Cunha, and P. Rogério Pinto Rodrigues, "Nb_2O_5 synthesis and characterization by Pechini method to the application as electron transport material in a solar device," *Sol. Energy*, vol. 216, pp. 1–6, Mar. 2021, doi: 10.1016/ J.SOLENER.2021.01.029.

[19] P. Viswanathamurthi, N. Bhattarai, H.Y. Kim, D.R. Lee, S.R. Kim, and M.A. Morris, "Preparation and morphology of niobium oxide fibres by electrospinning," *Chem. Phys. Lett.*, vol. 374, no. 1–2, pp. 79–84, Jun. 2003, doi: 10.1016/S0009-2614(03)00702-4.

[20] M.V. Reddy, R. Jose, A. Le Viet, K.I. Ozoemena, B.V.R. Chowdari, and S. Ramakrishna, "Studies on the lithium ion diffusion coefficients of electrospun Nb_2O_5 nanostructures using galvanostatic intermittent titration and electrochemical impedance spectroscopy," *Electrochim. Acta*, vol. 128, pp. 198–202, May 2014, doi: 10.1016/J.ELECTACTA.2013.10.003.

[21] J.Y. Cheong *et al.*, "Mesoporous orthorhombic Nb_2O_5 nanofibers as pseudocapacitive electrodes with ultra-stable Li storage characteristics," *J. Power Sources*, vol. 360, pp. 434–442, Aug. 2017, doi: 10.1016/J.JPOWSOUR.2017.06.030.

[22] P. Du *et al.*, "TiO_2/Nb_2O_5 core–sheath nanofibers film: Co-electrospinning fabrication and its application in dye-sensitized solar cells," *Electrochem. commun.*, vol. 25, no. 1, pp. 46–49, Nov. 2012, doi: 10.1016/J.ELECOM.2012.09.013.

[23] L. Wang, Y. Li, and P. Han, "Electrospinning preparation of g-C_3N_4/Nb_2O_5 nanofibers heterojunction for enhanced photocatalytic degradation of organic pollutants in water," *Sci. Reports 2021 111*, vol. 11, no. 1, pp. 1–12, Nov. 2021, doi: 10.1038/s41598-021-02161-x.

[24] L. Wang, Y. Li, P. Han, and Y. Jiang, "Facile fabrication of Fe-doped Nb_2O_5 nanofibers by an electrospinning process and their application in photocatalysis," *RSC Adv.*, vol. 11, no. 1, pp. 462–469, Dec. 2020, doi: 10.1039/D0RA10042K.

[25] N.C. Hildebrandt, J. Soldat, and R. Marschall, "Layered Perovskite Nanofibers via Electrospinning for Overall Water Splitting," *Small*, vol. 11, no. 17, pp. 2051–2057, May 2015, doi: 10.1002/SMLL.201402679.

[26] E.T. de Jesus *et al.*, "Potential of Nb_2O_5 nanofibers in photocatalytic degradation of organic pollutants," *Environ. Sci. Pollut. Res.*, vol. 28, no. 48, pp. 69401–69415, Dec. 2021, doi: 10.1007/S11356-021-15435-8/FIGURES/10.

[27] A. Radoń *et al.*, "Catalytic activity of non-spherical shaped magnetite nanoparticles in degradation of Sudan I, Rhodamine B and Methylene Blue dyes," *Appl. Surf. Sci.*, vol. 487, pp. 1018–1025, Sep. 2019, doi: 10.1016/J.APSUSC.2019.05.091.

[28] R.C. Carvalho, M.E.V. Mendonça, M.S. Tavares, E. Moreira, and D.L. Azevedo, "Optoelectronic and thermodynamic properties, infrared and Raman spectra of NbO_2 and Nb_2O_5 from DFT formalism," *J. Phys. Chem. Solids*, vol. 163, p. 110549, Apr. 2022, doi: 10.1016/J.JPCS.2021.110549.

[29] M. Ristić, S. Popović, and S. Musić, "Sol–gel synthesis and characterization of Nb_2O_5 powders," *Mater. Lett.*, vol. 58, no. 21, pp. 2658–2663, Aug. 2004, doi: 10.1016/J.MATLET.2004.03.041.

[30] D. Cao, W. Cai, W. Tao, S. Zhang, D. Wang, and D. Huang, "Lactic Acid Production from Glucose Over a Novel Nb_2O_5 Nanorod Catalyst," *Catal. Letters*, vol. 147, no. 4, pp. 926–933, Apr. 2017, doi: 10.1007/S10562-017-1988-6.

[31] H.T. Kreissl *et al.*, "Structural Studies of Bulk to Nanosize Niobium Oxides with Correlation to Their Acidity," *J. Am. Chem. Soc.*, vol. 139, no. 36, pp. 12670–12680, Sep. 2017, doi: 10.1021/JACS.7B06856.

[32] L. Kong, C. Zhang, J. Wang, W. Qiao, L. Ling, and D. Long, "Nanoarchitectured Nb_2O_5 hollow, Nb_2O_5@carbon and NbO_2@carbon Core-Shell Microspheres for Ultrahigh-Rate Intercalation Pseudocapacitors," *Sci. Reports 2016 61*, vol. 6, no. 1, pp. 1–10, Feb. 2016, doi: 10.1038/srep21177.

[33] M. Thommes *et al.*, "Physisorption of gases, with special reference to the evaluation of surface area and pore size distribution (IUPAC Technical Report)," *Pure Appl. Chem.*, vol. 87, no. 9–10, pp. 1051–1069, Oct. 2015, doi: 10.1515/PAC-2014-1117.

[34] L. Lou *et al.*, "Facile fabrication of interconnected-mesoporous T-Nb_2O_5 nanofibers as anodes for lithium-ion batteries," *Sci. China Mater. 2018 624*, vol. 62, no. 4, pp. 465–473, Sep. 2018, doi: 10.1007/S40843-018-9338-6.

[35] G. Li *et al.*, "Ethanol sensing properties and reduced sensor resistance using porous Nb_2O_5–TiO_2 n-n junction nanofibers," *Sensors Actuators B Chem.*, vol. 283, pp. 602–612, Mar. 2019, doi: 10.1016/J.SNB.2018.12.074.

[36] S. Qi, R. Zuo, Y. Liu, and Y. Wang, "Synthesis and photocatalytic activity of electrospun niobium oxide nanofibers," *Mater. Res. Bull.*, vol. 48, no. 3, pp. 1213–1217, Mar. 2013, doi: 10.1016/J.MATERRESBULL.2012.11.074.

[37] W. Li, R. Gao, M. Chen, S. Zhou, and L. Wu, "Facile synthesis and unique photocatalytic property of niobium pentoxide hollow spheres and the high optoelectronic performance of their nanofilm," *J. Colloid Interface Sci.*, vol. 411, pp. 220–229, Dec. 2013, doi: 10.1016/J.JCIS.2013.08.022.

[38] Y. Zhao *et al.*, "Shape-Dependent Acidity and Photocatalytic Activity of Nb_2O_5 Nanocrystals with an Active TT (001) Surface," *Angew. Chemie*, vol. 124, no. 16, pp. 3912–3915, Apr. 2012, doi: 10.1002/ANGE.201108580.

[39] C. Daza Gómez and J. Enrique Rodríguez-Páez, "The effect of the synthesis conditions on structure and photocatalytic activity of Nb_2O_5 nanostructures," *Process. Appl. Ceram.*, vol. 12, pp. 218–229, 2018, doi: 10.2298/PAC1803218G.

[40] G. Falk *et al.*, "Microwave-assisted synthesis of Nb_2O_5 for photocatalytic application of nanopowders and thin films," doi: 10.1557/jmr.2017.93.

[41] N.P. Ferraz *et al.*, "CeO2–Nb_2O_5 photocatalysts for degradation of organic pollutants in water," *Rare Met.*, vol. 39, no. 3, pp. 230–240, Mar. 2020, doi: 10.1007/S12598-019-01282-7.

[42] M.K. Silva, R.G. Marques, N.R. C.F. Machado, and O.A.A. Santos, "Evaluation of Nb_2O_5 and Ag/Nb_2O_5 in the photocatalytic degradation of dyes from textile industries," *Brazilian J. Chem. Eng.*, vol. 19, no. 4, pp. 359–363, 2002, doi: 10.1590/S0104-66322002000400001.